EPJ Web of Conferences **90**, 01005 (2015)
DOI: 10.1051/epjconf/20159001005

Particle correlations and their implication to collectivity in pPb and PbPb from CMS

Byungsik Hong[1,a] for the CMS Collaboration

[1] *Department of Physics, Korea University, Seoul 136-701, Republic of Korea*

Abstract. The long-range two-particle correlation functions reveal the near-side ridge structures in high-multiplicity pp, pPb and PbPb collisions at the Large Hadron Collider (LHC). The model that takes into account the collective flow originated from the initial-state geometry fluctuation can successfully describe the measured long-range correlation functions of charged particles. In this review paper, the recent experimental data on the long-range correlations and the extracted elliptic and triangular flow parameters in pPb and PbPb collisions from the Compact Muon Solenoid (CMS) experiment are summarized. The flow parameters from the long-range correlation analyses are compared with those from the multiparticle cumulants and the Lee-Yang Zeros (LYZ) method. In addition, the pseudorapidity dependence of long-range two-particle correlation functions in pPb and the deduced flow parameters for identified strange hadrons (K^0_S and $\Lambda/\bar{\Lambda}$) in pPb and PbPb are also presented to provide more insights on the long-range correlations and flow dynamics.

1 Introduction

The experiments at the Relativistic Heavy Ion Collider (RHIC) found the striking near-side ridge structure in the long-range two-particle correlations and the away-side conical emission in central AuAu collisions at 200 GeV of $\sqrt{s_{NN}}$ about a decade ago [1–3]. Naturally, the detailed study of the long-range two-particle correlation functions became one of the most interesting and urgent topics for the LHC heavy-ion program at higher energies. Soon after the LHC beams had been available, the ALICE, ATLAS, and CMS experiments observed near-side ridge and away-side conical emission structures by analyzing the first PbPb collision data at 2.76 TeV with much larger strengths [4–6]. Moreover, the CMS Collaboration also found the near-side ridge structure at the low transverse-momentum (p_T) region in violent pp events with the multiplicity larger than 110 [7], which has not been observed before in either hadron collisions or Monte-Carlo (MC) simulations.

The associated yield distributions for a short-range jet region ($|\Delta\eta|<1$) and the long-range ridge region ($2< |\Delta\eta| < 4$) for central 5% PbPb collisions are shown in Fig. 1 [8]. As expected, Fig. 1 shows that the jet-region yield increases with p_T^{trig} as the transverse energy of jet increases. On the contrary, the ridge-region yield becomes maximum for $2 < p_T^{trig} < 6$ GeV/c and decreases with p_T^{trig} and finally reaches almost zero at about 10 GeV/c. The PYTHIA8 MC simulations for pp, displayed by the solid lines in Fig. 1, are consistent with zero at all p_T^{trig} for the ridge-region yield and cannot describe the data at all.

[a] e-mail: bhong@korea.ac.kr

For pp collisions the multiplicity (N) dependence of the associated yields for the long-range near-side ridge region ($2< |\Delta\eta| < 4$) at 7 TeV is displayed in Fig. 2 [8]. The event sample for this analysis is selected for the momentum ranges of $2 < p_T^{trig} < 3$ GeV/c and $1 < p_T^{assoc} < 2$ GeV/c, where the near-side ridge effect is strongest. It is observed that the ridge effect turns on with $N \sim 50$ - 60 and shows a saturation around $N \sim 120$. However, this statement is not yet conclusive due to large statistical and systematic uncertainties.

There have been many attempts to explain the peculiar structures in the long-range two-particle correlation functions. Among them, the most successful scenario is the higher-order hydrodynamics flow induced by the geometric fluctuation of the overlapped region in initial stage [9], and this idea was successfully applied to the PbPb data at the LHC [8]. In this analysis, the one-dimensional $\Delta\phi$ projections of the two-particle correlation functions for relatively large pseudorapidity separation ($2 < |\Delta\eta| < 4$) are fitted by a Fourier series as

$$\frac{1}{N_{trig}}\frac{dN^{pair}}{d\Delta\phi} = \frac{N_{assoc}}{2\pi}\{1 + \sum_{i=1}^{\infty} 2V_{n\Delta}\cos(n\Delta\phi)\}, \quad (1)$$

where N_{assoc} is the number of charged hadron pairs per trigger particle in a given (p_T^{trig}, p_T^{assoc}) bin. Then, the extracted Fourier coefficients, $V_{n\Delta}$, can be factorized into the product of the single-particle harmonics, v_n, by

$$V_{n\Delta}(p_T^{trig}, p_T^{assoc}) = v_n(p_T^{trig}) \times v_n(p_T^{assoc}), \quad (2)$$

where $v_n(p_T^{trig})$ and $v_n(p_T^{assoc})$ represent the average azimuthal anisotropic harmonics for the triggered and asso-

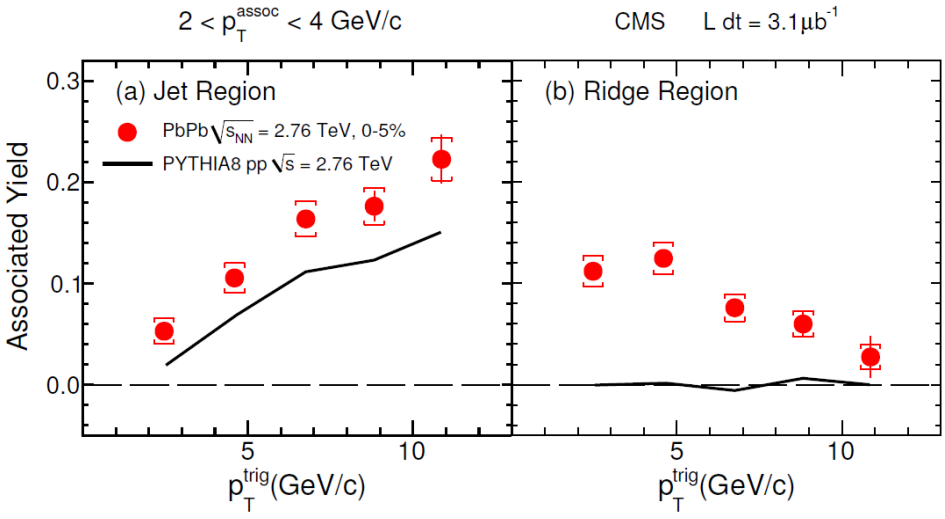

Figure 1. Integrated near-side associated yields as a function of p_T^{trig} for (a) the short-range jet region ($|\Delta\eta|<1$) and (b) the long-range ridge region ($2< |\Delta\eta| < 4$) [8]. The event samples are chosen for the most central 5% PbPb collisions at 2.76 TeV with $2 < p_T^{assoc} < 4$ GeV/c. The error bars represent the statistical uncertainties and the brackets around the symbols represent the systematic uncertainties. The solid lines are the calculations by PYTHIA8 of pp collisions at the same energy. The ridge-region yields are extracted by integrating the near-side long range $\Delta\phi$ correlation functions, and the jet-region yields are estimated by the difference between the short- and long-range near-side integrals.

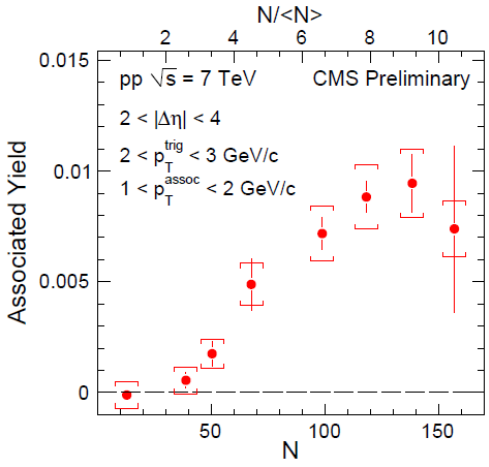

Figure 2. Integrated near-side associated yields for the long-range ridge region ($2< |\Delta\eta| < 4$) as a function of event multiplicity N [10]. The event samples are for $2 < p_T^{trig} < 3$ GeV/c and $1 < p_T^{assoc} < 2$ GeV/c in pp collisions at 7 TeV.

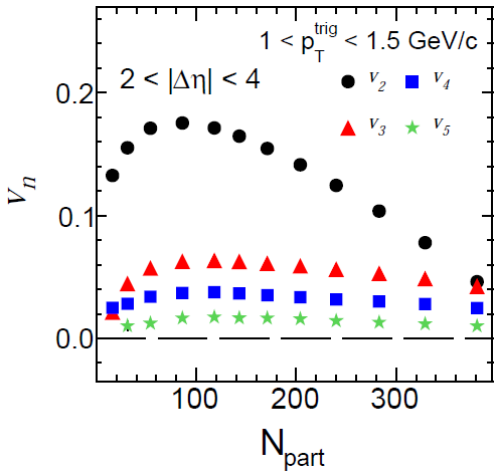

Figure 3. Single-particle harmonics, $v_2 \sim v_5$, extracted from the long-range two-particle azimuthal correlations as a function of the number of participant nucleons (N_{part}) in PbPb collisions at 2.76 TeV [10]. The chosen transverse-momentum ranges for the triggered and associated hadrons are $1 < p_T < 1.5$ GeV/c and $1 < p_T^{assoc} < 3$ GeV/c, respectively.

ciated particles [10]. One possible source of v_n is the collective flow arising from hydrodynamic expansion at low p_T. Figure 3 displays the single-particle harmonics, $v_2 \sim v_5$, extracted from the long-range two-particle correlation functions at low p_T as a function of the number of participant nucleons (N_{part}) in PbPb at 2.76 TeV [10]. The v_2 harmonics, sensitive to the eccentricity of the initial geometric configuration, becomes larger for peripheral collisions, but the higher-order harmonics, driven by fluctuation, display little dependence on the collision centrality.

This review paper summarizes the recent analysis results on the long-range dihadron correlations and the extracted flow harmonics in PbPb and pPb from CMS. In Sec. 2, the v_2 and v_3 single-particle harmonics deduced by the long-range two-particle correlation functions are compared with the results obtained by other methods like multiparticle cumulants and the LYZ method. Section 3 presents the pseudorapidity dependence of long-range two-particle correlation functions in pPb, and Sec. 4 decribes the v_2 and v_3 single-particle harmonics for K^0_S and $\Lambda/\bar{\Lambda}$ in pPb and PbPb. Finally, the summary in given in Sec. 5.

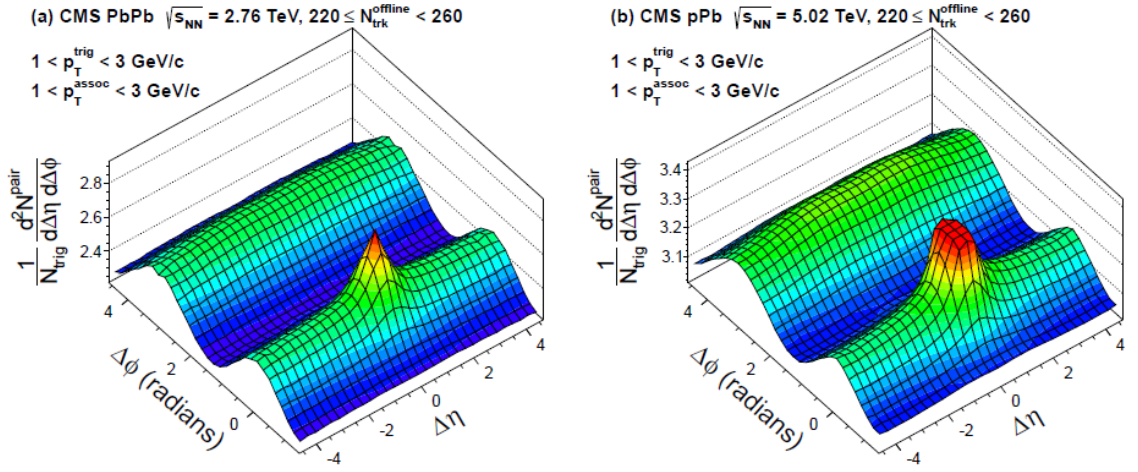

Figure 4. Two-dimensional two-particle correlation functions for (a) PbPb at 2.76 TeV and (b) pPb at 5.02 TeV [11]. The analyzed multiplicity range of 220 ≤ $N_{trk}^{offline}$ < 260, is same for PbPb and pPb collisions, and the transverse-momentum range of 1 < p_T < 3 GeV/c is same for the triggered and associated particles. The sharp near-side peaks for jets are truncated for better illustration of the long-range ridge structure.

2 Single-particle harmonics v_2 and v_3 in PbPb and pPb

Figure 4 displays the two-dimensional correlation functions in PbPb at 2.76 TeV and pPb at 5.02 TeV for charged particle pairs with 1 < $p_T^{trig/assoc}$ < 3 GeV/c [11]. The offline track multiplicity $N_{trk}^{offline}$ is defined as the measured number of primary tracks within $|\eta|$ < 2.4 and p_T > 0.4 GeV/c. In Fig. 4 the multiplicity condition of 220 ≤ $N_{trk}^{offline}$ < 260 is same for both collision systems, which corresponds to average centrality of ~60% for PbPb. For both PbPb and pPb, pronounced near-side long-range ridge structures are seen at $|\Delta\phi| \approx 0$. The near-side ridge structure in pPb at 5.02 TeV was also observed by ALICE and ATLAS [12, 13].

Figure 5 shows the integrated near-side associated yields as a function of p_T^{trig} for the long-range ridge region ($|\Delta\eta| > 2$) and the short-range jet region ($|\Delta\eta|<1$). In order to obtain the genuine jet yields, the long-range ridge components are subtracted for both collision systems in 220 ≤ $N_{trk}^{offline}$ < 260 [11]. It is observed that the estimated jet yields increase monotonically with p_T^{trig} similarly for PbPb and pPb collisions in the same multiplicity bin. In contrast, the long-range ridge yields increase with p_T^{trig}, reaching a maximum at $p_T^{trig} \approx$ 2 - 3 GeV/c, and gradually decrease at higher p_T^{trig} for both collisions. Moreover, the long-range ridge yields for PbPb are larger by almost a factor of two than those for pPb.

Using the method described by Eqs. 1 and 2, the single-particle second-order harmonic (v_2) coefficients are estimated from the long-range two-particle correlation functions for PbPb at 2.76 TeV and pPb at 5.02 TeV [14]. The open circles in Fig. 6 show the extracted v_2 values as a function of $N_{trk}^{offline}$ for 0.3 < p_T < 3.0 GeV/c. The $v_2\{2, |\Delta\eta| > 2\}$ values exhibit a moderate increase with $N_{trk}^{offline}$ in PbPb but remain relatively constant in pPb, especially, at high multiplicity. The magnitude of $v_2\{2, |\Delta\eta| > 2\}$ is found to be larger in PbPb than in pPb over a wide multiplicity range.

For comparison the v_2 values obtained by multiparticle cumulant correlations [15] and the LYZ method are also displayed in Fig. 6 [16]. In hydrodynamics, multiparticle correlations are arisen by anisotropic collective expansion originated from asymmetric initial geometry, and the corresponding Fourier coefficients v_n can be related to the correlation functions. On the other hand, the LYZ method involves correlations among all particles and is useful for the large-order behavior of the cumulant expansion for azimuthal correlations. Figure 6 shows that the $v_2\{2, |\Delta\eta| > 2\}$ values for both systems are consistently larger than those obtained by multiparticle cumulants and the LYZ method. This difference can be understood in hydrodynamic models since the event-by-event initial geometric fluctuations affect differently to the two-particle and multiparticle cumulant correlations. As a result, the $v_2\{2, |\Delta\eta| > 2\}$ values contain the residual nonflow correlation effects, and the multiparticle cumulant method has an advantage for providing cleaner collective signals compared to the two-particle correlation method [17]. The v_2 values from multiparticle cumulants and the LYZ method for PbPb increase with $N_{trk}^{offline}$, but those for pPb show little dependence on event multiplicity.

Figure 7 shows the single-particle third-order harmonic (v_3) coefficients as a function of $N_{trk}^{offline}$ for 0.3 < p_T < 3.0 GeV/c in PbPb at 2.76 TeV and pPb at 5.02 TeV obtained by the long-range two-particle correlation analysis [11]. The lines in Fig. 7 represent the extracted v_3 values after the low-multiplicity data with $N_{trk}^{offline}$ < 20 are subtracted for $V_{n\Delta}$ to get rid of the enhanced jet correlations coming from the preferential selection of high-multiplicity events. As this subtraction procedure usually affects the high-p_T region of low-multipicity events, $v_2\{2, |\Delta\eta| > 2\}$ and $v_3\{2, |\Delta\eta| > 2\}$ remain almost unchanged in the high-multiplicity region for $N_{trk}^{offline}$ > 200.

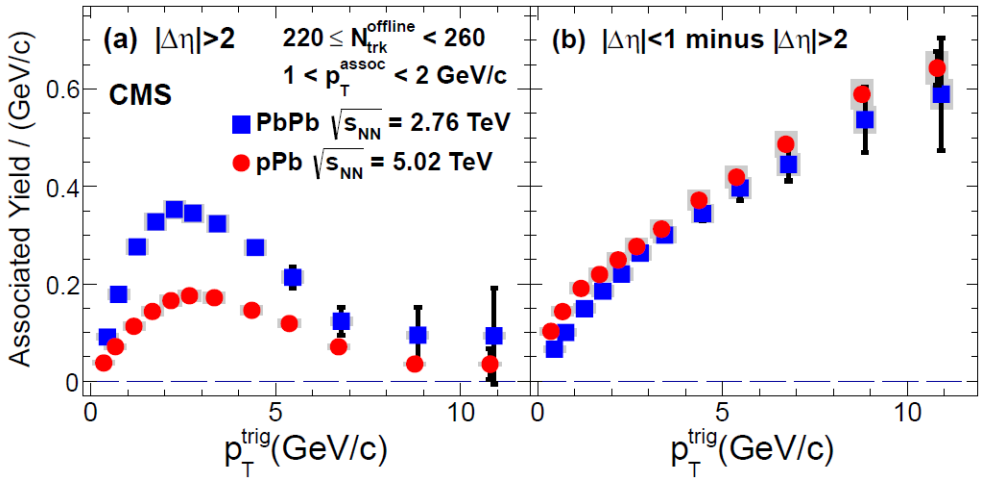

Figure 5. Integrated near-side associated yields as a function of p_T^{trig} for (a) the long-range ridge region ($|\Delta\eta| > 2$) and (b) the short-range jet region ($|\Delta\eta|<1$). For the short-range jet components in (b), the long-range ridge components are subtracted [11]. The multiplicity range of $220 \leq N_{trk}^{offline} < 260$ and the transverse-momentum range of $1 < p_T^{assoc} < 2$ GeV/c are same for PbPb and pPb collisions.

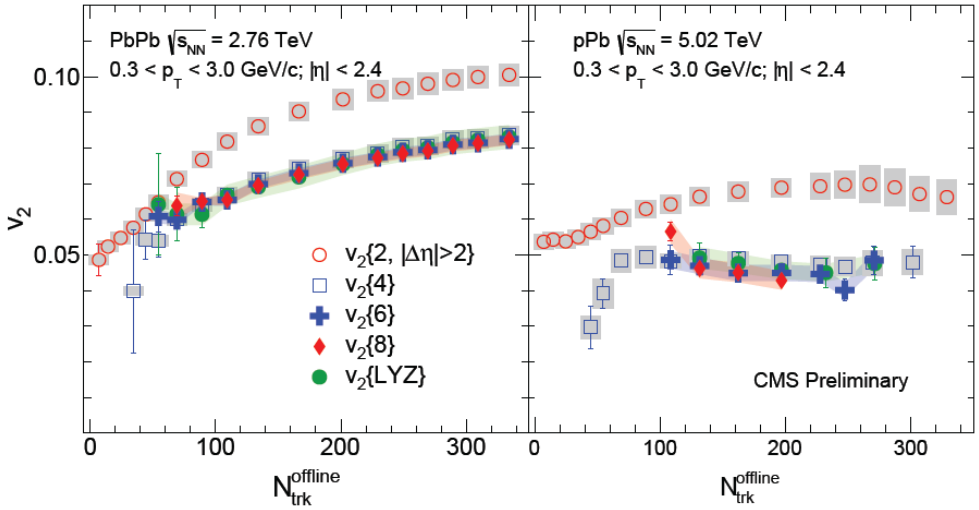

Figure 6. Single-particle second-order harmonic (v_2) coefficients for $0.3 < p_T < 3.0$ GeV/c as a function of $N_{trk}^{offline}$ in PbPb at 2.76 TeV (left) and pPb at 5.02 TeV (right), obtained by various analysis methods [14]. The open circles that are extracted by the long-range two-particle correlation functions [11] are compared with the results from multiparticle cumulant correlations and the LYZ method [14].

Note that the $v_3\{2, |\Delta\eta| > 2\}$ values for low-multiplicity pPb events in Fig. 7 become larger after the subtraction because the $V_{3\Delta}$ values for $N_{trk}^{offline} < 20$ are negative. Unlike $v_2\{2, |\Delta\eta| > 2\}$ shown in Fig. 6, the magnitude of $v_3\{2, |\Delta\eta| > 2\}$ is similar for PbPb and pPb in the same event multiplicity bin. This similarity of the triangular flow is non-trivial phenomenon within hydrodynamic picture because the initial-state geometry is quite different for the two collision systems.

3 Pseudorapidity dependence of long-range correlations in pPb

In order to gain further insights into long-range correlation in pPb, the $\Delta\eta$ dependent analysis has been performed by limiting the trigger particles to a narrow η ranges [18]. The near-side correlated ridge yields for high-multiplicity ($220 < N_{trk}^{offline} < 260$) pPb events are shown in Fig. 8 as a function of the pseudorapidity of the associated particle η_{assoc}. Here, the variable η_{assoc} is defined by the sum of $\Delta\eta$ and $\langle\eta_{trig}\rangle$, the mean η value of trigger particles. The two chosen η windows for trigger particles are $-2.4 < \eta_{trig} < -2.0$ for Pb-going-side trigger and $2.0 < \eta_{trig} < 2.4$ for p-going-side trigger. Figure 8 shows that the $\Delta\eta$ dependences of the near-side ridge yields are different for Pb-going-side and p-going-side triggers. For the Pb-going-side trigger, the ridge yield is larger when the two correlated particles are closer and decreases towards higher η_{assoc}. On the contrary, the ridge yield is almost independent of η_{assoc} for the p-going-side trigger.

The explanation of different η_{assoc} dependences for the two trigger conditions can be provided by hydrodynamic

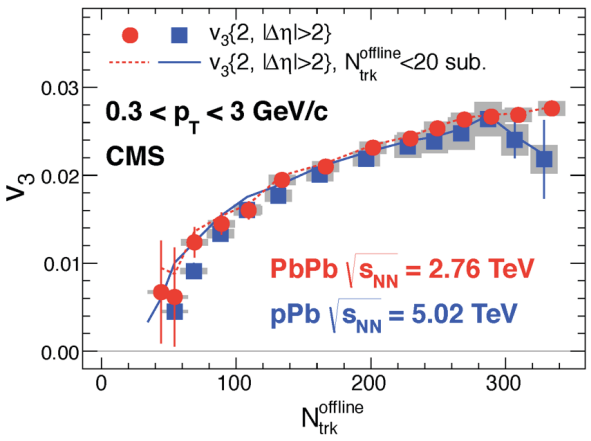

Figure 7. Single-particle third-order harmonic (v_3) coefficients as a function of $N_{trk}^{offline}$ for $0.3 < p_T < 3.0$ GeV/c in PbPb at 2.76 TeV (circles) and pPb at 5.02 TeV (squares) obtained from the long-range two-particle correlation analysis [11]. The solid and dotted lines represent the results after the low-multiplicity data for $N_{trk}^{offline} < 20$ are subtracted.

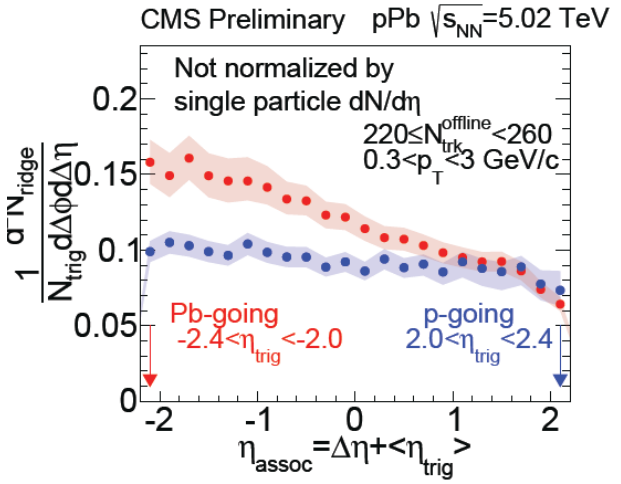

Figure 8. Near-side ridge yields for $0.3 < p_T^{trig/assoc} < 3$ GeV/c as a function of the associated particle's η, η_{assoc}, for high-multiplicity ($220 < N_{trk}^{offline} < 260$) pPb events [18]. The triggered η ranges are $-2.4 < \eta_{trig} < -2.0$ for the Pb-going-side trigger data (red) and $2.0 < \eta_{trig} < 2.4$ for the p-going-side trigger data (blue). The statistical errors are smaller than the symbol size, and the shaded bands represent systematic uncertainties.

flow. In hydrodynamic scenario, the ridge yield is related to the pair density per trigger particle of the underlying event. The η dependences of the ridge yields, shown in Fig. 8, are qualitatively in accordance with the $dN/d\eta$ distribution of the underlying event [19]. However, they differ quantitatively as the measured ridge yield can be described by the $dN/d\eta$ distribution of the underlying event multiplied by an additional linear function in $\Delta\eta$. The ridge yield distribution for pPb, discussed in Sec. 2, was uniform in $\Delta\eta$ because the correlations were integrated over a wide η range of the triggered particles. But Fig. 8 demonstrates that the ridge yield in pPb indeed depends on $\Delta\eta$.

Figure 9 shows the self-normalized single-particle anisotropy parameters, $v_2(\eta_{assoc})/v_2(0)$ and $v_3(\eta_{assoc})/v_3(0)$, obtained by Eqs. 1 and 2, as a function of η_{assoc} for high-multiplicity pPb events with $220 < N_{trk}^{offline} < 260$ at 5.02 TeV [18]. The circles Fig. 9 represent the triggered data after the low-multiplicity events with $N_{trk}^{offline} < 20$ are subtracted for $V_{n\Delta}$, whereas the lines show the data without subtraction. In Fig. 9 only the long-range data points with $|\Delta\eta| > 1$ are displayed, and a good agreemen between the two triggered data exist in the overlapped region. Significant η dependence of v_2 is observed as a larger decrease is observed in the p-going side. For triangular flow, finite v_3 is observed, but current large statistical uncertainties unfortunately prevent any definite conclusions on the η dependence.

4 Long-range correlations of K_S^0 and $\Lambda/\bar{\Lambda}$ in PbPb and pPb

To provide more insights on the particle production and expansion dynamics, long-range two-particle correlation functions have been studied for identified strange hadrons, K_S^0 and $\Lambda/\bar{\Lambda}$, in high-multiplicity pPb collisions with $220 < N_{trk}^{offline} < 260$ at 5.02 TeV [20]. In this analysis the pair of two tracks are assumed to be $\pi^+\pi^-$ in K_S^0 reconstruction and $\pi^- p$ ($\pi^+\bar{p}$) in Λ ($\bar{\Lambda}$) reconstruction [21]. Figure 10 shows the invariant-mass distributions of K_S^0 and $\Lambda/\bar{\Lambda}$ candidates with $1 < p_T < 3$ GeV/c for high-multiplicity pPb events ($220 < N_{trk}^{offline} < 260$) at 5.02 TeV [20]. The peaks for K_S^0 and $\Lambda/\bar{\Lambda}$ candidates are clearly identified with small backgrounds. Each peak is fitted by a double Gaussian function with a common mean, and the background distribution is fitted by the 4th-order polynomial function. The peak region is defined as the mass window of $\pm 2\sigma$ around the centeral value where σ is the standard deviation of the double Gaussian fit function. The amount of background in the peak region for the correlation measurement is estimated by the sideband region at least $\pm 3\sigma$ away from the central peak value.

Figure 11 shows the two-dimensional two-particle correlation functions for $K_S^0 - h^\pm$ and $\Lambda/\bar{\Lambda} - h^\pm$ pairs in high-multiplicity pPb events at 5.02 TeV [20]. In Fig. 11 the multiplicity range is $220 \leq N_{trk}^{offline} < 260$ and the transverse-momentum range is $1 < p_T < 3$ GeV/c for the triggered and associated particles. The two-particle correlation functions for $K_S^0 - h^\pm$ and $\Lambda/\bar{\Lambda} - h^\pm$ pairs show long-range ridge structures extending at least 4.8 units of $|\Delta\eta|$ in high-multiplicity pPb events. These ridge structures diminish for low-multiplicity events for $N_{trk}^{offline} < 35$.

The single-particle second-order harmonic (v_2) coefficients have been extracted for K_S^0 and $\Lambda/\bar{\Lambda}$ by using Eqs. 1 and 2. Figure 12 presents the v_2 values of K_S^0 and $\Lambda/\bar{\Lambda}$ as a function of p_T at several multiplicity bins for PbPb at 2.76 TeV and pPb at 5.02 TeV [20]. For comparison the v_2 data of unidentified charged particles ($h^\pm$) are also displayed. In the low-p_T region ($p_T \lesssim 2$ GeV/c) the v_2 data for K_S^0 are systematically larger than those for $\Lambda/\bar{\Lambda}$. However, the order is reversed at higher p_T region so that the v_2 data

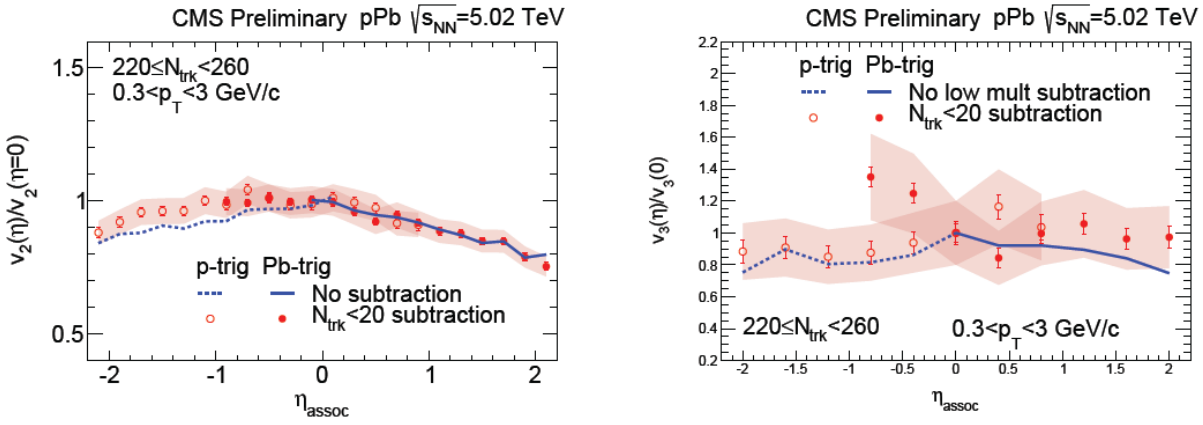

Figure 9. Self-normalized single-particle anisotropy parameters, $v_2(\eta_{assoc})/v_2(0)$ (left) and $v_3(\eta_{assoc})/v_3(0)$ (right), in $0.3 < p_T < 3.0$ GeV/c as a function of η_{assoc} for high-multiplicity pPb events ($220 < N_{trk}^{offline} < 260$) at 5.02 TeV [18]. The solid and open circles represent the Pb-going-side and the p-going-side triggers, respectively, after the low-multiplicity events ($N_{trk}^{offline} < 20$) are subtracted. The lines show the data without the subtraction.

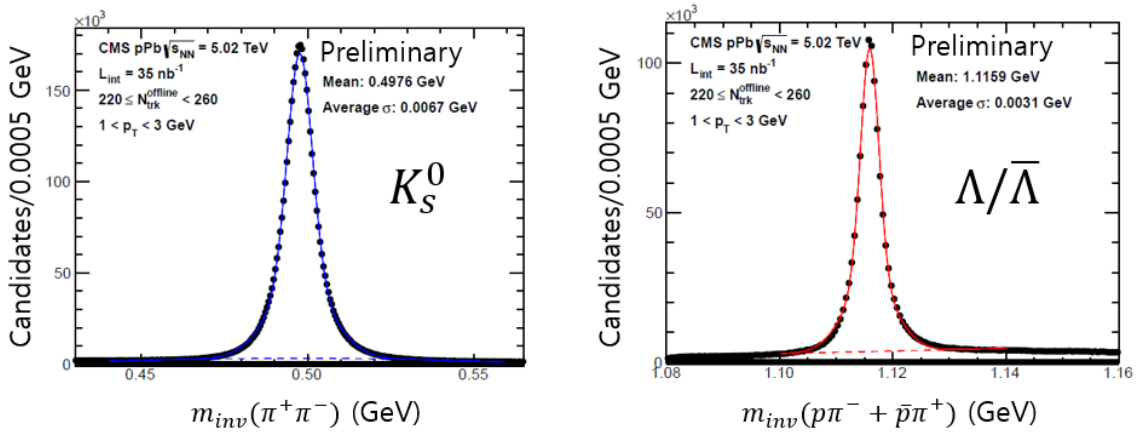

Figure 10. Invariant-mass distributions of K_S^0 (left) and $\Lambda/\bar{\Lambda}$ (right) candidates for high-multiplicity pPb events at 5.02 TeV [20]. The multiplicity range is $220 \leq N_{trk}^{offline} < 260$ and the transverse-momentum range is $1 < p_T < 3$ GeV/c for the triggered and associated particles. The solid line in each panel represents the fit function that is the sum of a double Gaussian for signal and the 4th-order polynomial for background.

for $\Lambda/\bar{\Lambda}$ are larger than those of K_S^0. In the meantime, the v_2 values of unidentified charged particles, mostly consisting of pions, consistently exceeds those of K_S^0 and $\Lambda/\bar{\Lambda}$ at $p_T \lesssim 2$ GeV/c, but falls between them for the two identified strange hadron species at $p_T \gtrsim 2$ GeV/c. The p_T dependences of v_2 are qualitatively similar for PbPb and pPb collisions in the same multiplicity bin. These observations indicate the mass-ordering effect and crossover of v_2 at $p_T \sim 2$ GeV/c.

Figure 13 presents the signle-particle third-order hamonic (v_3) coefficients for K_S^0 and $\Lambda/\bar{\Lambda}$ as a function of p_T for PbPb at 2.76 TeV and pPb at 5.02 TeV [20]. Due to the limited statistics the multiplicity range has been enlarged to $185 \leq N_{trk}^{offline} < 350$ for both systems. The p_T dependences of v_3 are found to be similar to those of v_2 for K_S^0 and $\Lambda/\bar{\Lambda}$. The mass-ordering effect and crossover at $p_T \sim 2$ GeV/c manifest also for v_3.

5 Summary

Since the first observation at RHIC almost a decade ago, understanding the origin of the near-side ridge structure in the long-range two-particle correlation functions has been prime interest in heavy-ion collisions at colliders. The LHC experiments measured much stronger ridge structure in PbPb collisions at 2.76 TeV. Furthermore, CMS found the near-side ridge structure at low transverse momenta even in high-multiplicity pp events, which is absent in hadron collision data as well as Monte-Carlo simulations. To provide more insights on the long-range two-particle correlations and flow harmonics, CMS analyzed the PbPb and pPb data at the LHC.

The integrated near-side associated yields for the long-range ridge region were analyzed as a function of transverse momentum in PbPb and pPb collisions for high-multipicity events. The long-range ridge yields increase with transverse momentum, reaching a maximum at 2-3

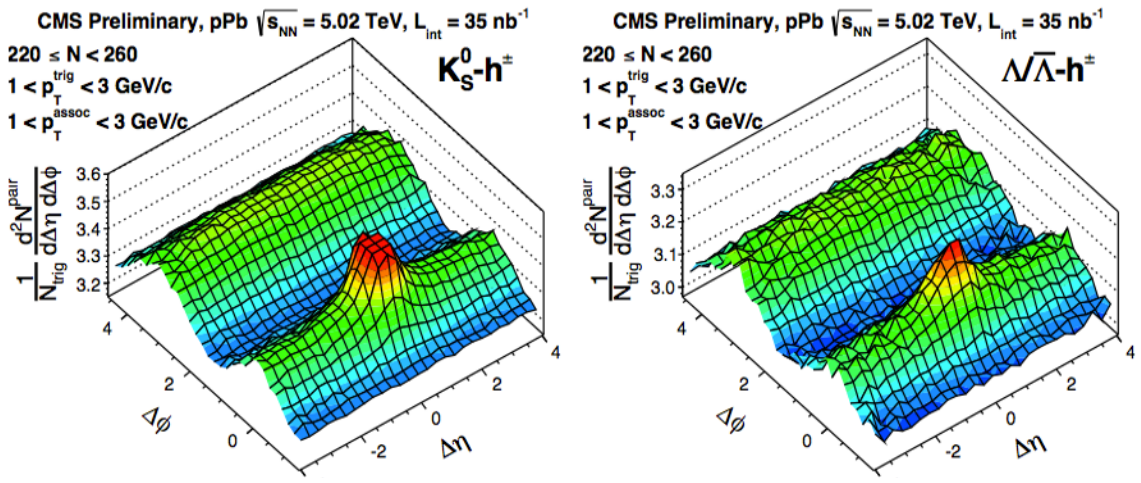

Figure 11. Two-dimensional two-particle correlation functions for $K^0_S - h^\pm$ (left) and $\Lambda/\bar{\Lambda} - h^\pm$ (right) pairs in high-multiplicity pPb events at 5.02 TeV [20]. The multiplicity range is $220 \le N^{offline}_{trk} < 260$ and the transverse-momentum range is $1 < p_T < 3$ GeV/c for the triggered and associated particles. The sharp near-side peaks for jets are truncated for better illustration of the long-range ridge structures.

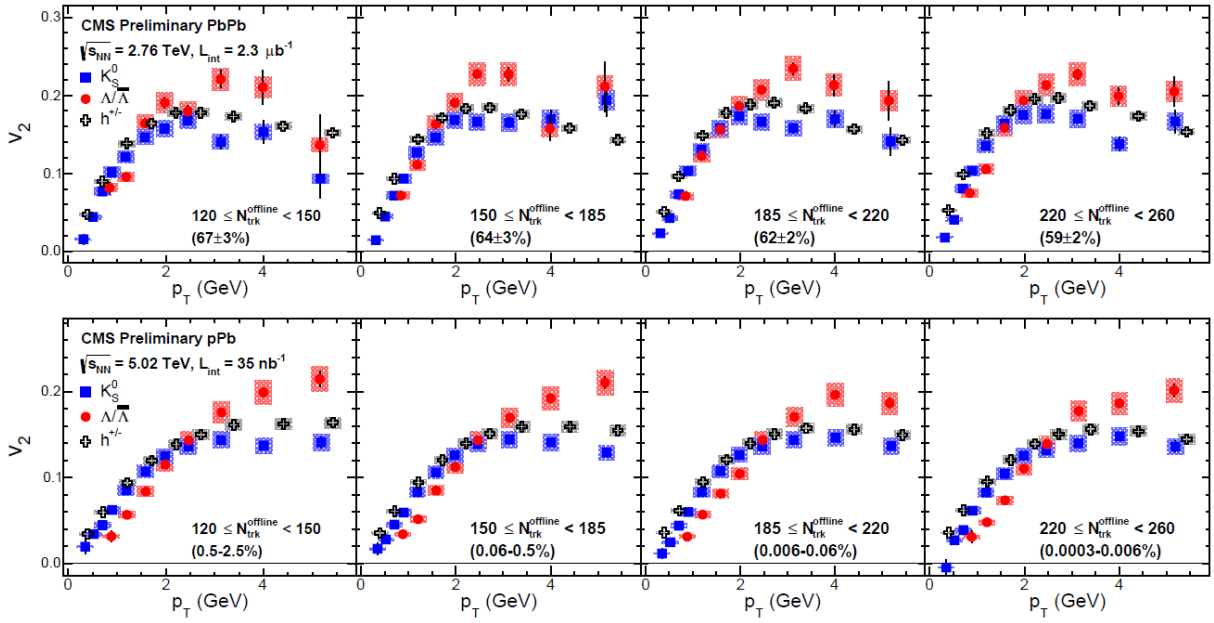

Figure 12. Single-particle second-order harmonic (v_2) coefficients extracted from the long-range correlation functions for K^0_S (squares), $\Lambda/\bar{\Lambda}$ (circles), and unidentified charged hadrons $h^\pm$ (crosses) as a function of p_T at different multiplicity bins [20]. The upper panels are for PbPb at 2.76 TeV and the lower panels are for pPb at 5.02 TeV.

GeV/c, and gradually decrease at higher transverse momentum for both systems. The single-particle second-order Fourier coefficients (v_2) were extracted from the long-range two-particle correlation functions. The v_2 data exhibit a moderate increase with multiplicity in PbPb but remain relatively constant in pPb, especially at high-multiplicity bins. The magnitude of v_2 is observed to be larger in PbPb than in pPb over a wide multiplicity range. The v_2 values from multiparticle cumulant correlations and the LYZ method were compared with the present data. The v_2 in PbPb increases with multiplicity, but that in pPb show little dependence on multiplicity. On the other hand, the single-particle third-order Fourier coefficients (v_3) is similar each other for PbPb and pPb in the same event multiplicity bin.

The pseudorapidity dependences of the near-side ridge yield and the single-particle Fourier coefficients were investigated by limiting the trigger particles to a narrow η range. The two η triggers for Pb-going and p-going sides were chosen. The long-range near-side ridge yields for high-multiplicity pPb events showed different η dependences for the two triggers. The ridge yield is larger when the two particles are closer and decreases towards higher η_{assoc} for the Pb-going-side trigger, but almost indepen-

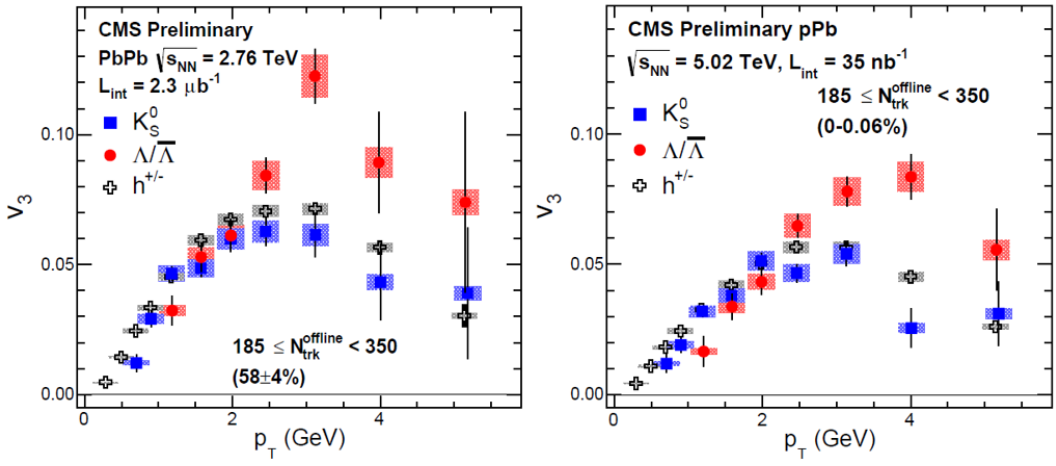

Figure 13. Single-particle third-order harmonic (v_3) coefficients extracted from the long-range correlation functions for K^0_S (squares), $\Lambda/\bar{\Lambda}$ (circles), and unidentified charged hadrons $h^{\pm}$ (crosses) as a function of p_T for PbPb at 2.76 TeV (left) and pPb at 5.02 TeV (right) [20]. The multiplicity condition, $185 \leq N^{offline}_{trk} < 350$, is the same for both systems.

dent of η_{assoc} for the p-going-side trigger. In the hydrodynamic scenario, the ridge yield is related to the pair density per trigger particle of the underlying event. The present data are qualitatively in accordance with the $dN/d\eta$ distribution of the underlying event.

Finally, the long-range two-particle correlation functions were analyzed for identified strange hadrons, K^0_S and $\Lambda/\bar{\Lambda}$, in PbPb and pPb. The two-dimensional two-particle correlation functions for $K^0_S - h^{\pm}$ and $\Lambda/\bar{\Lambda} - h^{\pm}$ pairs show long-range ridge structures extending more than 4.8 units of $|\Delta\eta|$ in high-multiplicity pPb events. The single-particle harmonics v_2 and v_3 were extracted for K^0_S and $\Lambda/\bar{\Lambda}$ for PbPb and pPb. The mass ordering and crossover of v_2 and v_3 at $p_T \sim 2$ GeV/c were observed: the v_2 and v_3 of K^0_S is systematically larger than those of $\Lambda/\bar{\Lambda}$ in the low p_T region at around 2 GeV/c, and vice versa at the higher p_T region.

Acknowledgements

This work was supported in part by the National Research Foundation of Korea (NRF) grant funded by the Korea government (MSIP) (No. 2008-00460) and Korea University.

References

[1] C. Zhang for the PHENIX Collaboration, Nucl. Phys. A **34**, S671 (2007)
[2] J. Putschke for the STAR Collaboration, Nucl. Phys. A **34**, S679 (2007)
[3] PHOBOS Collaboration, Phys. Rev. Lett. **104**, 062301 (2010)
[4] J. Jia for the ATLAS Collaboration, J. Phys. G **38**, 124012 (2011)
[5] J. F. Grosse-Oetringhaus for the ALICE Collaboration, J. Phys. G **38**, 124028 (2011)
[6] W. Li for the CMS Collaboration, J. Phys. G **38**, 124027 (2011)
[7] CMS Collaboration, J. High Energy Phys. **09**, 091 (2010)
[8] CMS Collaboration, J. High Energy Phys. **07**, 076 (2011)
[9] B. Alver and G. Roland, Phys. Rev. C **81**, 054905 (2010)
[10] CMS Collaboration, PAS HIN-11-006 (2011)
[11] CMS Collaboration, Phys. Lett. B **724**, 213 (2013)
[12] ALICE Collaboration, Phys. Lett. B **719**, 29 (2013)
[13] ATLAS Collaboration, Phys. Lett. B **725**, 60 (2013)
[14] CMS Collaboration, PAS HIN-14-006 (2014)
[15] A. Bilandzic, R. Snellings, and S. Voloshin, Phys. Rev. C **83**, 044913 (2011)
[16] R. S. Bhalerao, N. Borghini, and J. Y. Ollitrault, Nucl. Phys. A **727**, 373 (2003).
[17] J. Y. Ollitrault, A. M. Poskanzer, ans S. Voloshin, Phys. Rev. C **80**, 014904 (2009).
[18] CMS Collaboration, PAS HIN-14-008 (2014)
[19] ALICE Collaboration, Phys. Rev. Lett. **110**, 032301 (2013).
[20] CMS Collaboration, PAS HIN-14-002 (2014), submitted to Phys. Lett. B
[21] CMS Collaboration, J. High Energy Phys. **05**, 064 (2011)